Excitons in Photosynthesis

DOI: 10.1002/ange.201303231

Fluctuations in the Electron–Phonon Coupling of a Single Chromoprotein**

*Ralf Kunz, Kõu Timpmann, June Southall, Richard J. Cogdell, Arvi Freiberg, and Jürgen Köhler**

Since the determination of the X-ray structure of the peripheral light-harvesting complex, LH2, from the purple bacterium *Rhodopseudomonas* (*Rps.*) *acidophila*,[1,2] this pigment-protein complex has served as a cornerstone with which to elucidate the structure–function relationships that lie at the heart of the high efficiency of bacterial photosynthesis. This antenna complex accommodates 27 Bacteriochlorophyll (BChl) *a* molecules that are organized in two concentric rings, referred to as B800 and B850, according to the spectral positions of their absorption bands. Its structure has inspired many researchers, and convincing evidence was found that collective effects play an important role in the electronically excited states of the B850 manifold.[3–10] Yet, due to the heterogeneity in these systems, direct experimental confirmation of delocalized exciton states is difficult to obtain in conventional ensemble-averaged experiments, but was accomplished by single-molecule spectroscopy.[11] Apart from details that are still a matter of hot debate, it is now generally accepted that an exciton model that takes the heterogeneity in the site energies of the individual BChl *a* molecules into account grasps the essential features observed in absorption and fluorescence–excitation spectroscopy of LH2.[10,12,13]

There are several observations in the emission spectra that are inconsistent with this model, and this suggested a model that considers exciton self-trapping in the B850 assembly.[14–16] However, thus far, most of the single-molecule work performed on pigment-protein complexes from purple bacteria has focused on fluorescence–excitation spectroscopy, and the few studies that dealt with single-complex emission spectroscopy did not consider self-trapping processes[17–21] and/or were conducted at room temperature, where all decisive spectral details are completely masked by thermal broadening.[22–30] Recently, we addressed this issue by performing fluorescence–excitation and fluorescence spectroscopy on the same individual complex.[31] We found that, in contrast to the excitation spectra, the emission spectra could be grouped into three categories. Those that consist of a narrow zero-phonon line (ZPL), accompanied by a broader phonon side band (PSB) at lower energy, those that showed a broad structureless asymmetric band, and those that looked like a superposition of spectra from the former two categories. Moreover, we observed a clear correlation between the spectral peak position of the emission and the widths of the emission spectra. In agreement with selective spectroscopy data obtained from ensembles of LH2,[32,33] the complexes with emission spectra that featured a clear ZPL/PSB profile occurred preferentially on the blue side of the ensemble-averaged emission peak, and complexes with rather red-shifted spectra typically featured structureless broad bands. This observation clearly indicates that the electron–phonon coupling strength strongly varies from complex to complex, as well as being a function of the spectral position. Therefore, we came to the conclusion that exciton self-trapping might indeed be effective for some of the LH2 complexes emitting at the red end of the spectrum. At that time, the minimum exposure time for recording an individual emission spectrum from a single complex was 60 s and we could not fully rule out that some of the broader spectra were the result of fast spectral diffusion processes smearing out the underlying ZPL/PSB profile.

Herein, we describe our investigations of single LH2 complexes with a significantly improved spectral resolution and, more importantly, a reduction of the exposure time for recording an emission spectrum by using improved CCD technology. We find that spectral diffusion does indeed play a role, but, more interestingly, we also observed that the electron–phonon coupling strengths within an individual complex vary strongly as a function of time. The spectral features and correlations for a single complex are similar to those we found before for the variations between different individual complexes. As the electron–phonon coupling strength can be associated with the displacement of the equilibrium positions of the nuclei upon photoexcitation of the chromophore assembly, these findings are of direct relevance for the degree of exciton delocalization within the B850 states.

In Figure 1a we present a stack of 1000 consecutively recorded emission spectra from a single LH2 complex in

[*] R. Kunz, Prof. Dr. J. Köhler
Experimental Physics IV and Bayreuth Institute for Macromolecular Research (BIMF), University of Bayreuth
95440 Bayreuth (Germany)
E-mail: juergen.koehler@uni-bayreuth.de
Homepage: http://www.ep4.phy.uni-bayreuth.de
Dr. K. Timpmann, Prof. Dr. A. Freiberg
Institute of Physics, University of Tartu
Tartu EE-51014 (Estonia)
J. Southall, Prof. Dr. R. J. Cogdell
College of Medical, Veterinary and Life Sciences, University of Glasgow, Glasgow G12 8QQ (Scotland, UK)

[**] R.K. and J.K. gratefully acknowledge financial support from the Deutsche Forschungsgemeinschaft (KO 1359/16-1, GZ: 436 EST 113/4/0-1 and GRK1640) and the State of Bavaria within the initiative "Solar Technologies go Hybrid". K.T. and A.F. have been partially supported by the Estonian Research Council (IUT02-28). R.J.C. thanks the BBSRC for financial support. We thank Prof. M. van Heel (Imperial College London, UK) for providing us with the MSA algorithm.

Supporting information for this article is available on the WWW under http://dx.doi.org/10.1002/anie.201303231.

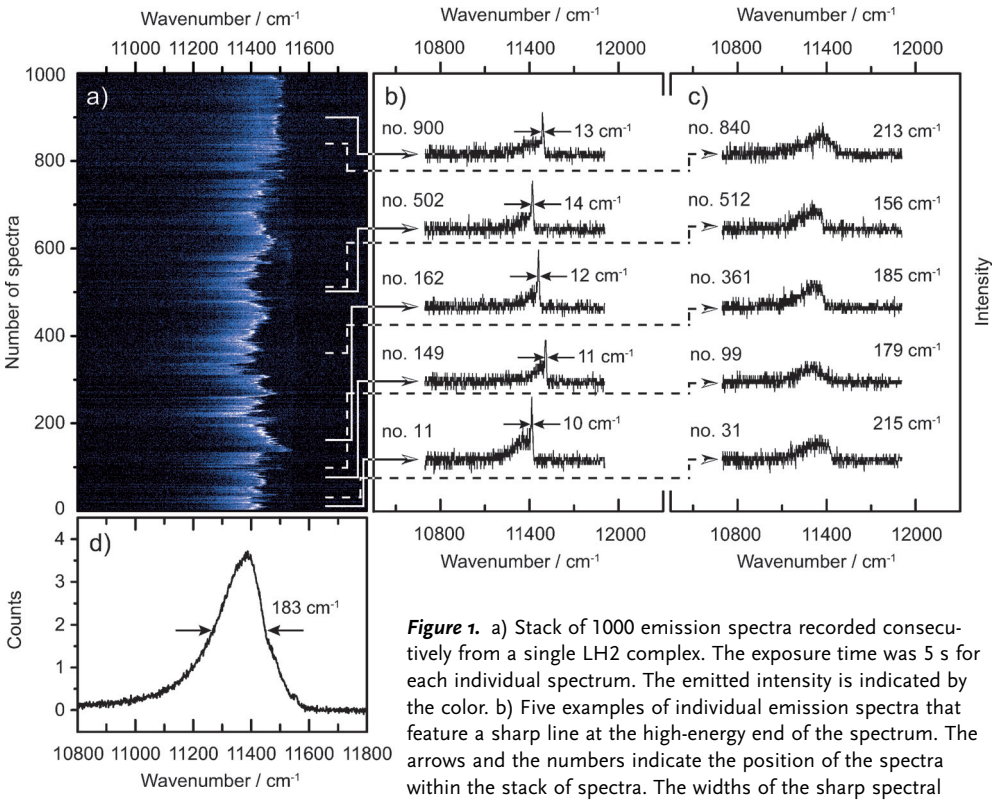

Figure 1. a) Stack of 1000 emission spectra recorded consecutively from a single LH2 complex. The exposure time was 5 s for each individual spectrum. The emitted intensity is indicated by the color. b) Five examples of individual emission spectra that feature a sharp line at the high-energy end of the spectrum. The arrows and the numbers indicate the position of the spectra within the stack of spectra. The widths of the sharp spectral features are given by the numbers next to the spectra and have been determined to within (± 1 cm^{-1}). c) Five examples of individual emission spectra with a broad structureless profile. The arrows and the numbers indicate the position of the spectra within the stack of spectra. The widths of the bands are given by the numbers next to the spectra. For clarity, all spectra in (b) and (c) are offset with respect to each other. d) Sum of all 1000 emission spectra. Note the different scales for the abscissae in (a)and (d) with respect to (b) and (c).

a two-dimensional representation (see also the movie in the Supporting Information). The horizontal axis corresponds to the emission energy and the vertical axis indicates the number of individual spectra, each one recorded with an exposure time of 5 s. From the spectral trail displayed in Figure 1 a, we extracted ten examples of individual spectra, which are shown in Figure 1 b,c. The spectra are grouped according to their spectral profiles. On the left hand side (Figure 1 b), the individual spectra feature a sharp zero-phonon line (ZPL) at the high-energy end of the spectrum, and a spectrally broad phonon side band (PSB) at lower energies. The full width at half maximum (FWHM) of the ZPLs varies from 10 cm^{-1} to 15 cm^{-1}. Although these linewidths are the smallest ever observed in the emission of LH2, this is still far broader than the homogeneous linewidth of about 0.005 cm^{-1} (150 MHz) that one would expect from the lifetime of the first excited singlet state.[16,34,35] The contributions to the linewidths that exceed the finite spectral resolution of about 7 cm^{-1} probably reflect unresolved spectral diffusion. In contrast, the spectra on the right side (Figure 1 c) appear as asymmetric broad bands with a width in the order of 150–200 cm^{-1}. We cannot rule out that these profiles are still influenced by spectral fluctuations on time scales faster than 5 s. In both cases, the arrows that connect the spectra with the pattern in Figure 1 a indicate the position of the example spectrum within the stack of spectra. Apparently, both types of spectral profiles appear randomly in time from the same single complex. These subtle details that are present in the individual spectra are completely masked in the time-averaged sum spectrum that is shown in Figure 1 d. It features an asymmetric profile with a width of 183 cm^{-1} (FWHM) and peaks at 11 386 cm^{-1}. Given the spectral trail displayed in Figure 1 a, it is clear that both the shape and the width of the sum spectrum are heavily affected by spectral diffusion.

This example shows that a more quantitative analysis of the spectral profile of the time-averaged sum spectrum of many consecutively recorded emission spectra is prevented by the strong spectral diffusion. To extract emission spectra with a reasonable signal-to-noise ratio from the data, we applied a multivariate pattern recognition algorithm.[36,37] These algorithms are used to reconstruct the three dimensional structure of large biomolecules from two-dimensional projections that have been obtained by cryo-electron microscopy.[38,39] We have previously demonstrated that such algorithms can be successfully exploited for spectroscopy to retrieve the optical spectra from individual objects in disordered hosts.[40–43] Briefly, the spectra are grouped into a predetermined number of classes by pattern recognition techniques. This is achieved by maximizing the interclass variance and minimizing the intraclass variance (in a mathematical, least squares sense). Subsequently, the spectra assigned to the same class are averaged, which yields the class-averaged spectra (CAS). In other words, only spectra that are sufficiently similar are averaged.[36] This method eliminates all contributions to line broadening from spectral diffusion that are slower than the exposure time of 5 s.

The bar graph in Figure 2 shows the number of individual spectra that contributed to a distinct CAS as a function of the spectral peak position of the CAS for the example presented in Figure 1. The distribution is surrounded by examples of CAS that are arranged from left to right, according to their spectral peak position from red to blue. The CAS on the blue side allow for a clear distinction between the ZPL and the PSB. Moving across from the blue to the red side, the intensity distribution between the ZPL and the PSB gradually changes until the narrow feature becomes invisible and an asymmetric band is observed for the emission spectra.

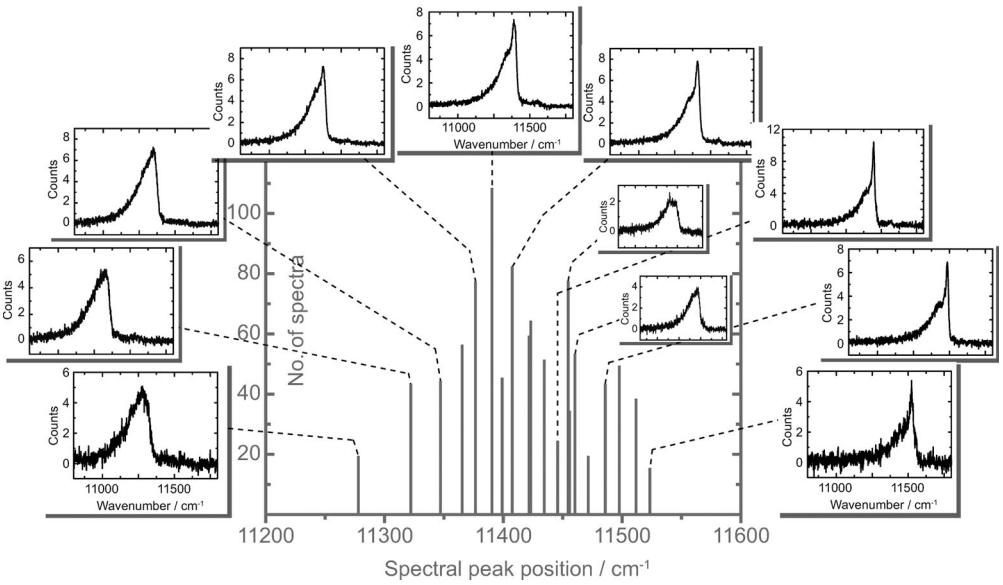

Figure 2. Distribution of the spectral peak position of the 20 class-averaged spectra (CAS). This analysis is based on a multivariate statistical pattern recognition algorithm (see text for details) and has been performed with the data shown in Figure 1 a. The vertical axis corresponds to the number of individual spectra that have contributed to a distinct class. The bar graph is surrounded by examples of CAS.

The general trend is that spectra with distinctive ZPLs are predominantly blue shifted with respect to the averaged emission maximum, whereas spectra with a broad structureless band appear predominantly at the red end. This correlation is illustrated in Figure 3, which shows the widths of the CAS (taken as FWHM, regardless of the spectral profile), as a function of the spectral peak position. As can be seen, there are no entries in this graph in the lower left corner and only a few entries in the top right corner. Examples for CAS that qualify for the latter case are shown in the inset of the main figure, and it is argued that these spectral profiles might be the result of unresolved fast spectral diffusion.

Further examples of CAS from individual complexes are presented in Figure 4 a. It shows the sum spectrum (black) together with the two CAS that feature the most blue- and red-shifted emission peaks for seven individual complexes. For an easier comparison, the most blue- and red-shifted CAS from the example shown in Figure 2, are reproduced as example **1**. Extreme examples for complexes that feature only little variation of the spectral profile of their emission spectra are **2** and **3**. For the spectra from example **2**, both CAS feature a clear ZPL and a PSB, and the spectral separation between the two emission peaks amounts to 94 cm^{-1}. In contrast, for example **3**, both the red-most and the blue-most CAS appear as structureless asymmetric bands. Here the spectral separation amounts to 135 cm^{-1}.

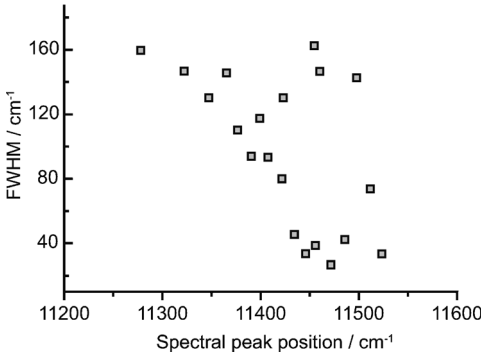

Figure 3. Spectral widths (FWHM) of the CAS presented in Figure 2 as a function of the spectral peak positions.

In total, we studied 26 LH2 complexes and, owing to the improved temporal and spectral resolution, the observed degree of heterogeneity (spectral profiles, fluctuations of the emitted intensity, spectral diffusion behavior, and magnitude of the spectral jumps) is far larger than previously observed by us.[31] Figure 4 b displays the widths of the two most spectrally separated CAS (blue and red) as a function of their spectral peak position for all complexes studied. For better visibility, the CAS from the same individual complex are connected by a straight line. This reveals that for each individual complex the width of the red-most CAS is always larger than the width of the blue-most CAS, whatever the actual profile of the emission spectrum looked like. As shown in Figure 4 c, the distribution of the spectral separations between the two extreme CAS is rather broad and covers the range from some 10 cm^{-1} to 350 cm^{-1}.

Such spectral jumps have been observed previously, either directly in room temperature experiments that allowed for recording sequences of spectra with short exposure times,[24] or as line broadening in experiments at cryogenic temperatures, where the signals were integrated over 1–10 min.[17,18] Given the low fluorescence quantum yield of LH2 (ca. 10 %), the optical excitation of the complex leads to an increase of the local temperature in the protein environment due to radiationless dissipation of excitation energy. Therefore, it is likely that the fluctuations of the electron–phonon coupling strength reflect light-induced conformational changes of the complex. As the spectral jumps and the connected spectral

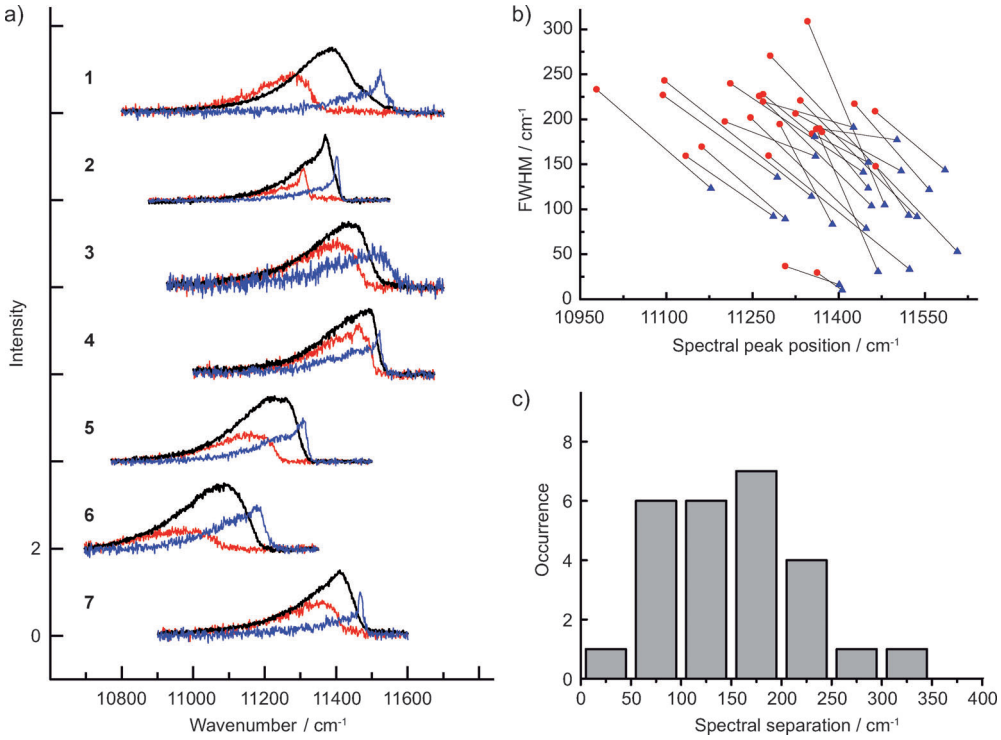

Figure 4. a) Examples of the most blue- and red-shifted CAS (blue and red, respectively) and the sum of all recorded emission spectra (black) for seven individual LH2 complexes. The blue CAS are peak normalized, and the red CAS are normalized such that the intensity ratio between the two CAS from the same complex is conserved. The sum spectra are peak normalized to 150% of the peak of the corresponding blue CAS for better visibility. Spectra that belong to different complexes have been offset with respect to each other for clarity. Example **1** was used for illustrations in Figures 1 and 2, and its spectra are reproduced here for comparison. b) Spectral widths (FWHM) of the most red-shifted (●) and the most blue-shifted CAS (▲) as a function of the spectral peak position. As a guide for the eye, CAS that belong to the same complex have been connected by a straight line. c) Distribution of the spectral separations between the most blue- and red-shifted CAS from the same complex.

profiles are reversible, we exclude deterioration of the complexes.

Given that the spectral separation between the most blue and most red emission spectra is on average around 150 cm^{-1}, which roughly corresponds to the thermal energy at room temperature (200 cm^{-1}), it can be expected that the lineshape fluctuations will be much faster at room temperature, which, together with thermal broadening effects, prevents the observation of distinctly different emission profiles. Although it was found that spectral jumps were well correlated with a broadening of the emission profile under ambient conditions. However, this correlation was both positive and negative; that is, broadening of the spectrum was observed for both spectral jumps to the blue and spectral jumps to the red.[24,27] To explain these time-averaged spectral envelopes, simulations using a modified Redfield theory were performed. There it was postulated that distinct conformations of the protein environment induce two different site energies for each individual pigment within the B850 assembly.[28,29] However, this model failed to explain the extreme spectral fluctuations and so it was later generalized to a four-state model, including two additional extremely blue- and red-shifted site energies for each pigment.[30] Thereby, the red-shifted realizations were associated with exciton self-trapping and a concomitant degree of exciton localization. Our experiments directly visualize the fluctuations of the electron–phonon coupling strength within a single pigment-protein complex and demonstrate that the LH2 ensemble emission spectrum should not be regarded as static. For each individual complex that contributes to it, there is a continuous movement of the spectral peak position accompanied by a change of the spectral profile. Emissions at the red end of the spectrum are dominated by contributions of broad featureless individual spectra, whereas the blue end of the spectrum predominantly consists of a superposition of ZPL/PSB-type spectral profiles. This might explain the inconsistencies that have been observed in absorption and emission studies on ensembles of LH2 concerning the electron–phonon coupling strength.[15]

In summary, we have registered emission spectra from individual LH2 complexes from *Rps. acidophila* at low temperature. Even for an individual complex, drastic fluctuations of the spectral profile were found and the correlation between the shape and the peak position of the emission spectrum provides direct evidence for strong fluctuations of the electron–phonon coupling strength. This demonstrates that conclusions about the B850 electronic excitations based on fluorescence–excitation spectroscopy on the one hand, and emission spectroscopy on the other, should be compared only with great care.[27] Fluorescence–excitation spectroscopy monitors the exciton wavefunction when it is "born". In contrast, emission spectroscopy provides information about the decay of the exciton, which might have undergone a temporal development, particularly if the electron–phonon coupling strength is fluctuating. This distinction is important for the correct interpretation of subsequent energy transfer reactions.

Experimental Section

Sample preparation was carried out as described in [31]. Briefly, LH2 complexes from *Rps. acidophila* (strain 10050, stored at −80°C) were diluted in buffer solution (20 mM Tris/HCl, pH 8.0, 0.1% LDAO) to

concentrations of about 10^{-11} M. In the last dilution step, 1.8% (wt/wt) polyvinyl alcohol (PVA; $M_w = 30000$–$70000\ g\,mol^{-1}$) was added and a small drop of the solution was spin-coated onto a quartz substrate. The samples were then mounted in a helium bath cryostat and cooled to 1.2 K. For the optical experiments, the samples were illuminated with a continuous-wave tuneable titanium-sapphire (Ti:Sa) laser (3900S, Spectra Physics) pumped by a frequency-doubled continuous-wave neodymium-yttrium-vanadate (Nd:YVO_4) laser (Millennia Vs, Spectra Physics) using a home-built microscope. First, a wide-field image of the sample was taken by exciting the sample through a band-pass filter (BP 858/30; Dr. Hugo Anders) at ca. 855 nm. The emission was collected by a microscope objective (NA = 0.85, Mikrothek) that was mounted inside the cryostat. After passing a set of band-pass filters (BP 900/50, AHF-Analysetechnik) the signal was reflected by a mirror that was mounted on the turret inside a spectrometer (SpectraPro-150, Acton Research Corporation) and focused onto a back-illuminated CCD camera (iKon-M DU934N-BR-DD, Andor Technology). Next, spatially well-isolated complexes were selected from the wide-field image and the fluorescence–excitation spectra of these complexes were registered.[31] Finally, the complex under study was excited in the B800 spectral region. To do so, the laser light passed a band-pass filter (BP 805/60; AHF Analysetechnik) and the wavelength was wobbled across one (or more) of the sharp B800 absorptions determined before. The polarization was kept fixed and the excitation intensity was about $1\ kW\,cm^{-2}$. The emitted light was directed through a set of long-pass filters (LP 830, AHF Analysetechnik), and, by rotating the turret in the aforementioned spectrometer, dispersed by a grating (600 lines/mm) to provide a spectral resolution of about $7\ cm^{-1}$. For each complex, 100–2000 emission spectra were repetitively recorded by accumulating the emission for 3–15 s on the same CCD camera, as mentioned above. All spectra displayed have been corrected for the spectral instrument response.

Received: April 17, 2013
Revised: May 22, 2013
Published online: July 3, 2013

Keywords: excitons · light-harvesting complexes · photosynthesis · single-molecule studies

[1] G. McDermott, S. M. Prince, A. A. Freer, A. M. Hawthornthwaite-Lawless, M. Z. Papiz, R. J. Cogdell, N. W. Isaacs, *Nature* **1995**, *374*, 517 – 521.
[2] M. Z. Papiz, S. M. Prince, T. Howard, R. J. Cogdell, N. W. Isaacs, *J. Mol. Biol.* **2003**, *326*, 1523 – 1538.
[3] T. V. Dracheva, V. I. Novoderezhkin, A. P. Razjivin, *FEBS Lett.* **1996**, *387*, 81 – 84.
[4] R. Monshouwer, R. van Grondelle, *Biochim. Biophys. Acta Bioenerg.* **1996**, *1275*, 70 – 75.
[5] K. Sauer, R. J. Cogdell, S. M. Prince, A. A. Freer, N. W. Isaacs, H. Scheer, *Photochem. Photobiol.* **1996**, *64*, 564 – 576.
[6] R. G. Alden, E. Johnson, V. Nagarajan, W. W. Parson, C. J. Law, R. J. Cogdell, *J. Phys. Chem. B* **1997**, *101*, 4667 – 4680.
[7] M. Chachisvilis, O. Kuehn, T. Pullerits, V. Sundström, *J. Phys. Chem. B* **1997**, *101*, 7275 – 7283.
[8] H.-M. Wu, M. Rätsep, I.-J. Lee, R. J. Cogdell, G. J. Small, *J. Phys. Chem. B* **1997**, *101*, 7654 – 7663.
[9] V. Sundström, T. Pullerits, R. van Grondelle, *J. Phys. Chem. B* **1999**, *103*, 2327 – 2346.
[10] X. Hu, T. Ritz, A. Damjanovic, F. Autenrieth, K. Schulten, *Q. Rev. Biophys.* **2002**, *35*, 1 – 62.
[11] A. M. van Oijen, M. Ketelaars, J. Köhler, T. J. Aartsma, J. Schmidt, *Science* **1999**, *285*, 400 – 402.
[12] H. van Amerongen, L. Valkunas, R. van Grondelle, *Photosynthetic Excitons*, World Scientific, Singapore, **2000**.
[13] R. J. Cogdell, A. Gall, J. Köhler, *Q. Rev. Biophys.* **2006**, *39*, 227 – 324.
[14] T. Polívka, T. Pullerits, J. L. Herek, V. Sundström, *J. Phys. Chem. B* **2000**, *104*, 1088 – 1096.
[15] K. Timpmann, Z. Katiliene, N. W. Woodbury, A. Freiberg, *J. Phys. Chem. B* **2001**, *105*, 12223 – 12225.
[16] A. Freiberg, M. Rätsep, K. Timpmann, G. Trinkunas, W. N. Woodbury, *J. Phys. Chem. B* **2003**, *107*, 11510 – 11519.
[17] C. Tietz, O. Cheklov, A. Dräbenstedt, J. Schuster, J. Wrachtrup, *J. Phys. Chem. B* **1999**, *103*, 6328 – 6333.
[18] W. P. F. de Ruijter, J. M. Segura, R. J. Cogdell, A. T. Gardiner, S. Oellerich, T. J. Aartsma, *Chem. Phys.* **2007**, *341*, 320 – 325.
[19] U. Gerken, F. Jelezko, B. Götze, M. Branschädel, C. Tietz, R. Ghosh, J. Wrachtrup, *J. Phys. Chem. B* **2003**, *107*, 338 – 343.
[20] U. Gerken, D. Lupo, C. Tietz, J. Wrachtrup, R. Ghosh, *Biochemistry* **2003**, *42*, 10354 – 10360.
[21] D. Uchiyama, H. Oikawa, K. Otomo, M. Nango, T. Dewa, S. Fujiyoshi, M. Matsushita, *Phys. Chem. Chem. Phys.* **2011**, *13*, 11615 – 11619.
[22] M. A. Bopp, A. Sytnik, T. D. Howard, R. J. Cogdell, R. M. Hochstrasser, *Proc. Natl. Acad. Sci. USA* **1999**, *96*, 11271 – 11276.
[23] S. Tubasum, R. J. Cogdell, I. G. Scheblykin, T. Pullerits, *J. Phys. Chem. B* **2011**, *115*, 4963 – 4970.
[24] D. Rutkauskas, R. Novoderezkhin, R. J. Cogdell, R. van Grondelle, *Biochemistry* **2004**, *43*, 4431 – 4438.
[25] D. Rutkauskas, J. Olsen, A. Gall, R. J. Cogdell, C. N. Hunter, R. van Grondelle, *Biophys. J.* **2006**, *90*, 2463 – 2474.
[26] D. Rutkauskas, V. Novoderezhkin, A. Gall, J. Olsen, R. J. Cogdell, C. N. Hunter, R. van Grondelle, *Biophys. J.* **2006**, *90*, 2475 – 2485.
[27] V. I. Novoderezhkin, D. Rutkauskas, R. van Grondelle, *Biophys. J.* **2006**, *90*, 2890 – 2902.
[28] L. Valkunas, J. Janusonis, D. Rutkauskas, R. van Grondelle, *J. Lumin.* **2007**, *127*, 269 – 275.
[29] J. Janusonis, L. Valkunas, D. Rutkauskas, R. van Grondelle, *Biophys. J.* **2008**, *94*, 1348 – 1358.
[30] V. I. Novoderezhkin, D. Rutkauskas, R. van Grondelle, *Chem. Phys.* **2007**, *341*, 45 – 56.
[31] R. Kunz, K. Timpmann, J. Southall, R. J. Cogdell, A. Freiberg, J. Köhler, *J. Phys. Chem. B* **2012**, *116*, 11017 – 11023.
[32] K. Timpmann, M. Rätsep, C. N. Hunter, A. Freiberg, *J. Phys. Chem. B* **2004**, *108*, 10581 – 10588.
[33] A. Freiberg, M. Rätsep, K. Timpmann, G. Trinkunas, *Chem. Phys.* **2009**, *357*, 102 – 112.
[34] T. J. Pflock, S. Oellerich, J. Southall, R. J. Cogdell, G. M. Ullmann, J. Köhler, *J. Phys. Chem. B* **2011**, *115*, 8813 – 8820.
[35] A. Freiberg, M. Rätsep, K. Timpmann, *Biochim. Biophys. Acta Bioenerg.* **2012**, *1817*, 1471 – 1482.
[36] L. Borland, M. van Heel, *J. Opt. Soc. Am. A* **1990**, *7*, 601 – 610.
[37] M. van Heel, B. Gowen, R. Matadeen, E. V. Orlova, R. Finn, T. Pape, D. Cohen, H. Stark, R. Schmidt, M. Schatz, A. Patwardhan, *Q. Rev. Biophys.* **2000**, *33*, 307 – 369.
[38] P. Dube, M. Wieske, H. Stark, M. Schatz, J. Stahl, F. Zemlin, G. Lutsch, M. van Heel, *Structure* **1998**, *6*, 389 – 399.
[39] P. Dube, E. V. Orlova, F. Zemlin, M. van Heel, J. R. Harris, J. Markl, *J. Struct. Biol.* **1995**, *115*, 226 – 232.
[40] C. Hofmann, H. Michel, M. van Heel, J. Köhler, *Phys. Rev. Lett.* **2005**, *94*, 195501.
[41] R. Hildner, U. Lemmer, U. Scherf, M. van Heel, J. Köhler, *Adv. Mater.* **2007**, *19*, 1978 – 1982.
[42] R. Hildner, L. Winterling, U. Lemmer, U. Scherf, J. Köhler, *ChemPhysChem* **2009**, *10*, 2524 – 2534.
[43] J. Baier, M. Gabrielsen, S. Oellerich, H. Michel, M. van Heel, R. J. Cogdell, J. Köhler, *Biophys. J.* **2009**, *97*, 2604 – 2612.

